Large, Controllable Spikes of Magnetoresistance in $La_{2/3}Ca_{1/3}MnO_3/SrTiO_3$ Superlattices

Sergey A. Fedoseev,[†] Alexey V. Pan,[†,*] Sergey Rubanov,[‡] Igor A. Golovchanskiy,[†] and Olga V. Shcherbakova[†]

[†]Institute for Superconducting and Electronic Materials, University of Wollongong, Northfields Avenue, Wollongong, NSW 2522, Australia and [‡]Electron Microscope Unit, Bio21 Institute, University of Melbourne, VIC 3010, Australia

ABSTRACT We have investigated superlattices consisting of up to 30 epitaxial nanomultilayers (3−7 nm thick) of ferromagnetic $La_{2/3}Ca_{1/3}MnO_3$ (LCMO) and insulating $SrTiO_3$ (STO) hybrids. The superlattices demonstrate dramatic shifts of Curie temperature, indicating the possibility of its tunability. The metal−insulator transition (MIT) has been observed around 140 K. Below the MIT temperature, the superlattices have shown sharp drops of resistivity, facilitating the largest and sharpest magnetoresistance peaks (>2000%) ever observed in LCMO films and superlattices at low temperatures. The observed experimental results can be explained in the frame of the phase separation model in manganites with well-organized structures. The results of magnetic and transport measurements of such hybrid structures are discussed, indicating a magnetodielectric effect in STO interlayers. The magnetic and transport properties of the superlattices are shown to be technology-dependent, experiencing dimensional transitions, which enables the creation of structures with prescribed magnetoresistance characteristics for a broad range of applications.

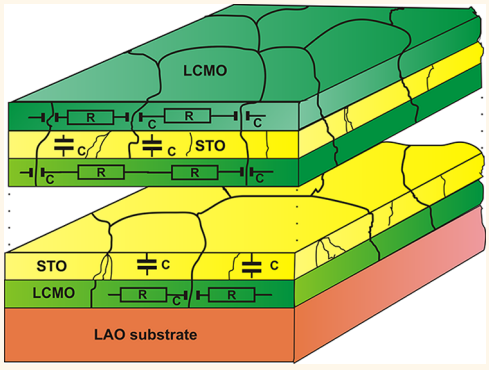

KEYWORDS: metal−insulator transition · thin film structure · LCMO/STO superlattice · magnetoresistance · 3D RC network

Perovskite manganite oxide, $La_{1-x}Ca_xMnO_3$, exhibits a great research interest due to the colossal magnetoresistance (CMR) observed in this material and a possibility to employ it for magnetic sensors, recording memory devices,[1,2] and emerging spintronic applications in the form of epitaxial films and heterostructures.[3,4] The key feature responsible for the CMR effect in this compound is the dynamic coexistence of phases with different properties, known as phase separation (PS).[5,6] The coexistence of insulating and metallic phases in $La_{2/3}Ca_{1/3}MnO_3$ (LCMO) was directly observed at temperatures below the Curie temperature (T_C).[7] In ref 8, the direct imaging of clusters with the size of around 3−4 nm was reported in lanthanum manganite and attributed to as evidence of the nanoscale phase separation. Moreover, manganite thin films exhibit unusual properties such as nonlinear resistance and resistance metastability.[9,10] However, the successful development of manganite-based devices requires certain magnetic and transport properties, in particular at surfaces and interfaces if hybrid heterostructures comprising cuprate and manganite components are used for spintronic applications employing CMR and high-temperature superconductivity (HTS).[11] Unfortunately, the lanthanum manganites usually demonstrate their relevant magnetic properties well above the superconducting critical temperature of the cuprates, which impairs the development of these hybrid applications.

Lower temperatures of the metal−insulator transition and the magnetoresistance enhancement at low temperatures were obtained by reducing the manganite film thickness[12] or by creating manganite−insulator superlattices with periods of $n \leq 10$.[13,14] However, no observations of unusual CMR behavior in these superlattices were reported below 90 K, the range of interest for combination with HTS materials.

In this work, we have grown $(LCMO/STO)_n$ superlattices (with n = 20−30 periods) on $LaAlO_3$ (LAO) substrates by pulsed laser deposition (PLD). To enhance effects observed, the thickness of individual LCMO

* Address correspondence to pan@uow.edu.au.

Received for review August 29, 2012 and accepted December 14, 2012.

Published online December 14, 2012
10.1021/nn304127n

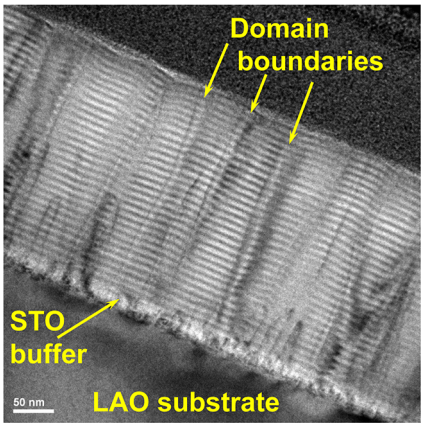

Figure 1. Typical transmission electron microscopy image of the cross section of (LCMO-3 nm/STO-3 nm)$_{30}$ superlattice grown on LAO substrate buffered with a 35 nm thick STO layer. Alternating bright and dark layers are STO and LCMO layers, respectively.

layers (~3 nm) is chosen to be comparable with the diameter of nanoclusters formed as a result of phase separation. We have investigated magnetic and transport properties of such superlattices and compared them with properties of LCMO films grown on similar substrates under the same technological conditions.

RESULTS AND DISCUSSION

Transmission electron microscopy shows sharp interfaces between LCMO and $SrTiO_3$ (STO) layers in LCMO/STO superlattices (SL). In Figure 1, the superlattice with (LCMO-3 nm/STO-3 nm)$_{30}$, hereafter denoted as SL4, is shown. The region in the vicinity of the substrate buffered by a 35 nm thick STO layer exhibits a high density of columnar defects, which evolve into a presumably more relaxed structure with 25−60 nm wide columnar domains characteristic of PLD epitaxial films. A similar structure has been observed for $REBa_2Cu_3O$ superconducting films and multilayers (RE denotes a rare earth element, such as Y or Nd).[15] The analysis of SEM images of the SL surfaces shows various rectangular patterns, from clearly separated rectangular islands of about 50 nm to the mosaics of interconnected chains of rectangular islands (as shown for SL4 in Figure 2) formed on the surface of the LCMO/STO superlattice depending on the structure, deposition conditions, and substrate selected. These rectangular surface features indicate the dimension (~50 nm) of the columnar domains. The columnar domains exhibit enhanced deformation (slightly enhanced upward layer curvature within domains) in the top half of the structure (Figure 1), which can result in rougher interfaces between the layers and eventually the surface itself. In the case of the SL4 shown in Figure 2, the surface is rather smooth with the roughness on the surface of about 10 nm as can be estimated from its lowest points at the boundaries to the highest points in the middle of the domains in Figure 1.

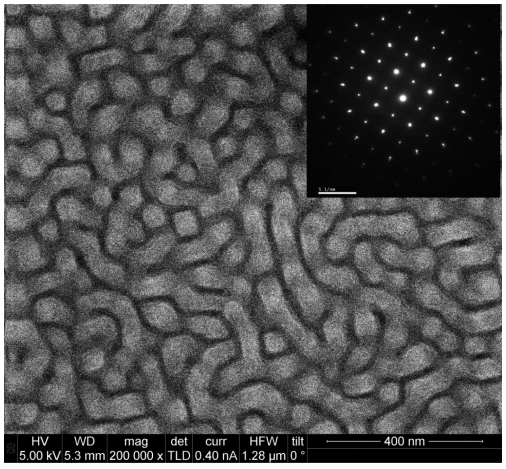

Figure 2. Field emission scanning electron microscopy (SEM) of the surface of (LCMO-3 nm/STO-3 nm)$_{30}$ superlattice, exhibiting the mosaic of interconnected chains of rectangular islands formed as a result of columnar growth. The diffraction pattern in the top right corner shows the cubic crystal structure of the epitaxially grown superlattice.

It is well-known that the boundaries between the columnar domains, traversing the entire thickness of the SL, disrupt the crystal structure and act as cumulative pinning centers for structural defects, such as edge dislocations.[16,17] These boundaries, marked by arrows in Figure 1, are usually 2−4 nm thick. On the other hand, the epitaxial growth of the cubic crystal structure in the superlattice is confirmed by the diffraction pattern in the inset of Figure 2. Thus, such columnar superlattices exhibit alternating sections of LCMO and STO with the average dimensions of 50 × 50 × 3 nm^3 each (or whatever the thickness of the layers is). This structure represents a 3D well-ordered mixed phase (or defined phase separation). Indeed, we consider the presence of two clearly defined, transversally alternating phases of LCMO and STO, as well as one or two minor in-plane phases serving as the domain boundaries. Obviously, we obtain a unique, well-organized 3D structure of alternating in-plane regions possessing high conductivity (crystalline LCMO) and low conductivity (STO and boundaries between columnar domains[21]). This structure can be well-controlled by selecting layer thickness and/or using various PLD deposition parameters and conditions, allowing one to obtain *controllable* structural properties of phase separation which governs the CMR effect.

The temperature dependence of magnetization [$M(T)$] for the zero-field-cooled (ZFC) samples with the in-plane field geometry is shown in Figure 3. The ferromagnetic Curie temperature for all measured samples has been estimated by finding the steepest slope from the temperature derivative of magnetization (dM/dT),[18,19] shown by arrows in Figure 3. It has been observed that, for single-layer LCMO films grown on LAO substrates, T_C is decreased with decreasing thickness of the layer. For the 200 nm thick LCMO film

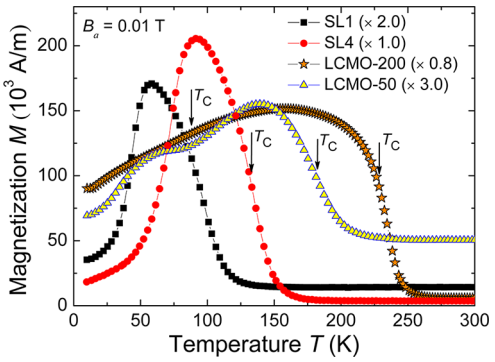

Figure 3. Temperature dependences of ZFC magnetization for LCMO films of 50 and 200 nm thick, as well as superlattices SL4 (LCMO-3 nm/STO-3 nm)$_{30}$ and SL1(LCMO-3 nm/STO-7 nm)$_{20}$ showing $T_C \simeq$ 180, 235, and 135, 74 K, respectively. Multipliers noted in the legend are applied to the corresponding curves for scaling.

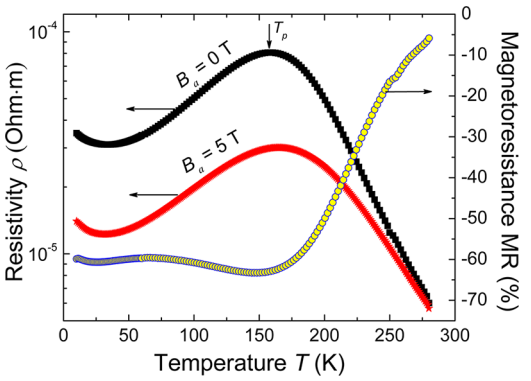

Figure 4. Temperature dependence of resistivity for the 50 nm thick LCMO film showing the MIT point (denoted by T_p) of about 160 K at zero and high applied magnetic fields. The magnetoresistance minimum is found also at around T_p.

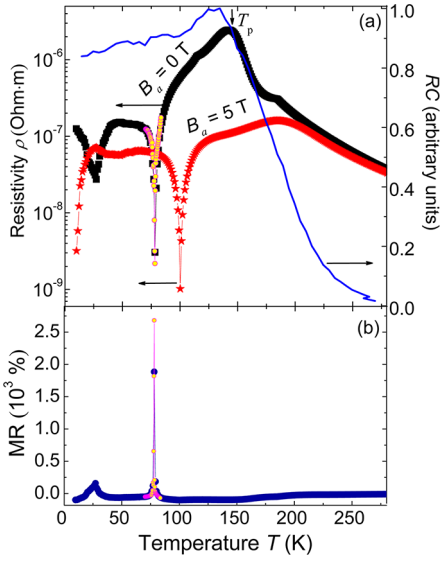

Figure 5. (a) Temperature dependence of resistivity of the SL4 superlattice grown on LAO substrate measured at B_a = 0 and 5 T. The solid line exhibits the temperature dependence of RC product (right axis) for LCMO/STO interface with $C(T)$ taken from ref 26 and $R(T)$ from Figure 4. (b) Magnetoresistance as a function of temperature shows two maxima at ≃27 and 75 K. Open circle curves overlapped in (a) and (b) show the reproducibility of the respective curves obtained by measuring with a smaller temperature step.

(LCMO-200), $T_C \simeq$ 235 K was obtained, whereas for the 50 nm thick film (LCMO-50) $T_C \simeq$ 180 K. This result is consistent with ref 12, which reported a similar trend for similar thickness reductions.

In contrast, we propose to effectively and dramatically control the T_C shift to lower temperatures by introducing a certain LCMO/STO superlattice structure grown on the same type of substrates. The SL1, which has a total LCMO thickness (~60 nm) similar to the 50 nm thick LCMO film, shows $T_C \simeq$ 74 K (Figure 3). The (LCMO-3 nm/STO-3 nm)$_{30}$ superlattice (SL4) with the total LCMO thickness of about 90 nm exhibits a correspondingly higher $T_C \simeq$ 134 K. Notably, as also follows from other measured (but not shown) superlattices, the thickness of STO layers may significantly affect the T_C trend. This change in properties of separated phases by the thickness of the STO interlayer is likely to support the phase separation as the mechanism responsible for the reduction of T_C with increasing insulating domains.[7]

We should note that some differences in the paramagnetic signals for our samples above T_C in Figure 3 are most likely due to different amounts of LCMO material, its architecture, and its possibe varying paramagnetic properties dependent on oxygen content.[19,20] In Figure 3, this difference was artificially enhanced due to the multipliers applied to the corresponding curves for scaling to improve presentation.

The transport measurements show significant differences between the temperature dependence of resistivity for the LCMO films and LCMO/STO superlattices. In Figure 4, resistivity (ρ) of the LCMO-50 film is shown as a function of temperature at the applied magnetic field B_a = 0 and 5 T. We can see a clear metal-to-insulator transition (MIT) at $T_p \simeq$ 160 K and metallic-like behavior below T_p. The temperature-dependent magnetoresistance (MR) for the same LCMO film is also shown in Figure 4. The MR is defined as MR = $[R(B_a) - R(0)] \times 100\%]/R(0)$, where $R(0)$ and $R(B_a)$ are the resistances at the applied field B_a = 0 and 5 T, respectively. The sample shows a MR minimum in the vicinity of the metal−insulator transition temperature. Both resistivity and MR behavior of the LCMO films measured are typical for the samples with similar thickness and composition as described in refs 9 and 10.

In the LCMO/STO superlattices (Figure 5a), the $\rho(T)$ behavior of the high-temperature paramagnetic part at $T > T_p$ is rather similar to the LCMO single-layer films. However, below T_p, the transport characteristics can be very different compared to the LCMO films of comparable thickness. The $\rho(T)$ curves for SL4 demonstrate two sharp singularities with the resistivity drops of up to 2 orders of magnitude for both zero-field and in-field resistivity curves. The corresponding magnetoresistance

curve is shown in Figure 5b for this superlattice. Above MIT temperature, the MR demonstrates behavior similar to single-layer LCMO films with negative MR values as high as −90%. Below T_p, the magnetoresistance of the superlattice shows two sharp *positive* peaks with the highest value of more than 2000% at $T \simeq 75$ K, which corresponds to the lowest resistivity point for the zero-field resistance dependence on temperature. Note that $\rho(T)$ curves are highly reproducible for every sample (as can be seen from two overlapped curves measured with different temperature step for the spike obtained at higher temperature) and do not have any dependence on cycles of cooling and heating. However, the behavior of spikes depends on the layer architecture and deposition parameters (including substrate selection). For example, for thicker STO interlayers (SL1) and fewer number of layers in the SL with very straight interfaces, even in the vicinity of the domain boundaries, no spikes have been observed; with a slight variation of the STO interlayer thickness (by <2 nm), the spikes' position can be adjusted; importantly, identical deposition conditions and layer architecture for different samples lead to identical behavior (verified during the refereeing process). The discussion of exact parameters allowing us to control the resistance drop behavior is outside the scope of this work and will be detailed elsewhere. In this work, we report this new phenomenon and its most pronounced behavior obtained for SL1 and SL4, as well as focus on its possible explanation.

The explanation of such unusual behavior can be proposed within the framework of a phase separation model, arising as a result of the well-ordered 3D alternating structure of ferromagnetic (FM) and insulating domains in our hybrid multilayered system (explained above).

According to the models of phase separation,[5,6] the concentration of carriers in various clusters (or system domains) affects the local and global magnetic properties[22] due to effective spin exchange through various mechanisms including double exchange, carriers (electron) hopping, crystal lattice distortions, *etc.*[23] In the paramagnetic state above the MIT temperature, spin-charge-ordered insulating phases create potential barriers between clusters (or domains) of ferromagnetic phase. The mutual phase charging due to increasing concentration of carriers leads to increasing Coulomb fields. This increase would expand conducting regions, eventually setting up presumably percolative conduction between them below the MIT at T_p. This does not destroy the phase separation but changes its topology,[6] most likely also within the LCMO domains.

Furthermore, below the MIT (Figure 5), two negative spikes in the resistivity curves have been observed in the superlattices for zero magnetic field and $B_a = 5$ T. The lower-temperature spike (at 27 K) is usually broader than the high-temperature spike (at 75 K). In addition, the spikes measured in the applied fields are shifted relative to their zero-field temperatures, so that the low-temperature spikes are observed at even lower temperatures, while the high-temperature spike is shifted to higher temperatures. It is also important to notice that the "background" resistivity does not drop substantially, remaining at the same level and likely indicating a similar mechanism of conductivity outside of the spike ranges. We presume that a certain degree of "tunneling" through structural barriers with high resistances between LCMO domains shown in Figure 2 is involved with marginal variations outside the spikes. Within the spike temperature range, the Coulomb potentials experience a progressive breakdown as the temperature of the sample is changed. The properties of multiple potential barriers created by the superlattices are expected to be temperature- and magnetic-field-dependent, which plays an important role in the progressive breakdown. This would mean that, instead of tunneling, the neighboring ferromagnetic regions become electrically connected, hence progressively lower resistivity is measured. As the Coulomb potentials discharge throughout the entire sample, the insulating barriers are again progressively reinstated, leading to reinstating resistivity and eventually to the "background" tunneling-driven percolative conductivity level. Both negative spikes may have a very similar scenario. However, the high-temperature spike at 75 K may have additional contribution from the out-of-plane tunneling barrier breakdown because of conducting filament formation (through the STO layers).[24] Thus, these two negative spikes may reflect characteristic behavior of the well-ordered domain structure (well-ordered PS) for in-plane (2D-like) and out-of-plane (3D-like) conductivity.

To illustrate the scenario described above, we propose the dimensional RC network model as follows. Taking into account that in our superlattice the LCMO semiconductor layers are separated by the insulating STO layers, a certain capacitance is created across each insulating layer. Thus, we can analyze a RC network in our superlattice with nonlinear, temperature-dependent resistors being represented by LCMO layers (Figure 6). The capacitor characteristics would depend on dielectric properties of STO layers, which in turn can also vary as a function of temperature and electric field strength. In Figure 5a, we reproduce the RC curve (solid line) obtained for a hybrid temperature dependence of a LCMO/STO interface capacitance (from ref 26) and a LCMO layer resistance from Figure 4. Indeed, the curve indicates substantial influence of the capacitance on the behavior observed in the superlattice. This approach should be reasonable for the STO interlayer thicknesses used in our SL because it was shown that even 0.8 nm thick STO layers can display good insulating properties.[25] However, the application of threshold voltages is likely to lead to the formation and rupture of filamentary conducting paths inside insulating

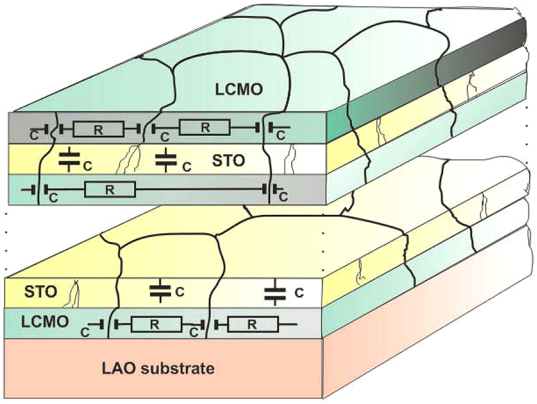

Figure 6. Model of LCMO/STO superlattice as the 3D RC network, where the formation of the filamentary conducting paths in the STO interlayers is shown as thin lightning bolt-like lines.

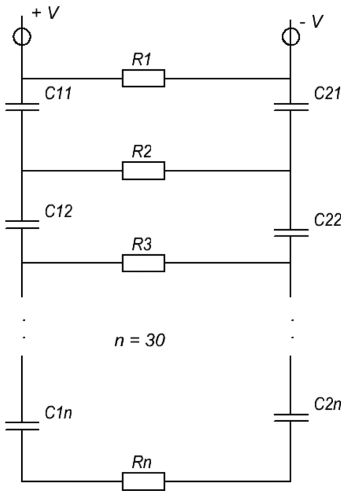

Figure 7. Simplified equivalent diagram of a superlattice with the assumption that all 2D-like in-plane resistances are within the LCMO layers with the in-plane capacitors across the LCMO domains being short-circuited, while the out-of-plane capacitors (across STO layers) effectively decouple the LCMO layers at and below the low-temperature negative spike where the capacitance would still be large to form conductive filament[24] (or breakdown) across the STO interlayers.

sublayers[24] (lightning bolt-like thin lines in STO layers in Figure 6), which respectively results in short-circuiting and reopening the capacitors.

In the situation where all of the in-plane capacitors (across the LCMO domain boundaries) are short-circuited presumably at the low-temperature negative spike, the RC network behaves as a set of 2D capacitively coupled resistors with the resistance R being determined by the in-plane LCMO resistance. The equivalent diagram of the RC network model is simplified in this case to the one shown in Figure 7.

At low temperatures (well below the low-temperature spike), the capacitance of the STO insulating layers is the highest,[26] hence the total resistance is likely defined by the 2D RC network of only one top LCMO layer (an ideal case) that is $R1 \simeq 1$ kΩ (measured at 10 K). As temperature increases, the relatively small capacitances across the LCMO domain boundaries breakdown, expanding electrically connected ferromagnetic clusters and decreasing the total 2D-like in-plane LCMO resistance. At the minimum of the low-temperature spike at $T_{m1} \simeq 27$ K (for zero field), the superlattice possesses the minimum resistance of $R1_{min} \simeq 80$ Ω at $I =$ 100 μA applied only to the top manganite layer.

At the minimum, the electric field strength between the voltage terminals has its minimal value $E \simeq 0.2$ V/m, which is too small for the connectivity filament formation, and the *inverse* process of filament rupture is triggered. Note that the local electric field strength between the LCMO domains across domain boundaries can be as high as hundreds of kV/m if we consider the width of the boundaries, which is on the order of a few nanometers.[15−17] It is sufficient to facilitate the capacitive domain boundary rapture.

Upon further increased temperature, we are expecting three processes to occur. (i) The capacitance of STO interlayers keeps degrading, which lowers the Schottky-like barrier and enables the formation of conducting filaments through STO layers.[26,27] (ii) A similar degradation process would be valid for the capacitance of the domain boundaries (reducing local electric field strengths), (iii) whereas the resistance of the LCMO within the domains keeps rising due to MIT (Figure 4), which redistributes E more evenly over the LCMO layers reducing the chance of the rupturing. This three-fold process can result in the behavior observed experimentally as follows.

The resistivity is rather constant between the two negative spikes, being the result of counteraction of rising resistivity within the LCMO domains, on one hand, and lowering capacitance of the domain boundaries, hence gradually enhancing the tunneling, on the other hand.

At a certain point, the capacitance *across the STO layer* drops below a threshold level (the onset of 3D-like behavior), so that it becomes favorable for carriers to tunnel through (or to rupture) the STO layers. As a result, a process similar to the 2D process described above for a single LCMO layer is initiated, but now it is likely to engage not only one LCMO layers but all LCMO layers for 2D in-plane conductance as well as tunneling or rupture of STO layers enabling the 3D-like participation of all LCMO layers. Again, a rough estimation of electric field across one ≃3−6 nm thick STO layer reaches $E \sim 2-4$ MV/m, which corresponds to the field strength necessary to rupture the STO layer of up to 1 μm thick.[27] According to our model, at the minimum of the spike at $T_{m2} = 78$ K, all capacitors across STO interlayers in Figure 7 have to be replaced by conducting filaments. This allows us to verify our model by a simple check of the total resistance *expected* at the minimum. It can be found by dividing the resistance of the single LCMO layer $R1 \simeq 80$ Ω measured at T_{m1} by

the number of the deposited LCMO layers in the SL4 (n = 30). Hence, the total network resistance expected at the minima of the spike is ~3 Ω. This value can be considered to agree well with the measured value of ≃15 Ω, in particular, if we recall that the resistance within LCMO domains rises with the temperature, while our estimation is based on the $R1$ value obtained at T_{m1} = 27 K. Furthermore, the disagreement may also be due to structural imperfections and short-circuiting between layers, which could also mean that $R1$ was measured as a parallel resistance of two (or even a few) LCMO layers, whereas we initially considered it an ideal case. Additionally, the resistance of the LCMO layers near the substrate may be quite different than the top layers due to the larger amount of defects in the initial layers near the substrate, as can be seen in TEM image (Figure 1).

At temperatures higher than T_{m2}, the reverse process commences due to the low averaged E value, in a fashion similar to that described above for the low-temperature spike. Eventually, the total superlattice resistance rises with temperature up to the MIT point.

Yet another confirmation of the dimensional mechanism proposed comes from the field dependence of the spike behavior. The first 2D low-temperature spike is proposed to be governed by in-plane FM domains. By applying an in-plane magnetic field, it forces the domains to align along the field, so that some neighboring domains are likely to merge, decreasing their number and increasing their size. This would lead to (i) a more rapid rupturing (and inverse) process (fewer domains), (ii) which is likely to happen at lower temperature, and (iii) resulting in a lower resistance at the minimum (fewer domain boundaries to rupture). Indeed, we observe these three features in our experiments (Figure 5a).

Furthermore, the second 3D high-temperature spike, on the contrary, shifts to a higher temperature at the applied field, which may confirm its different dimensionality as follows. Indeed, the dielectric properties of materials can be changed in materials, in general, and systems like the STO structure, in particular.[28,29] In our case, during the PLD process, STO interlayers in the superlattice may become doped (contaminated) with Mn or LCMO due to remnant plasma after switching targets from LCMO to STO, or/and the secondary ablation of LCMO upon STO deposition, or/and interdiffusion between layers at the deposition temperature of 780 °C. STO doped with Mn and LCMO itself has been shown to exhibit magnetodielectric effects.[30] This means that the dielectric constant of the STO interlayers would increase in the magnetic field applied, leading to the rupture process occurring at higher temperatures, as indeed was observed in our experiment at B_a = 5 T. Similarly to the first spike, because of the in-plane larger FM clusters, the rupture process would be more rapid, exhibiting lower resistance. These peculiarities are observed in our measurements (Figure 5a).

It is important to note that the resistivity of single-layer LCMO films in Figure 4 is higher than in the SL by 2 orders of magnitude, which is consistently observed for these types of SL. Intuitively, the resistance trend should have been reversed simply because the thicker conducting LCMO film had lower resistance than in the 2D LCMO layers of the SL separated by insulating STO. Indeed, although the total thickness of LCMO in the SL was kept equal to the corresponding single-layer LCMO films, the current was applied to the top layers only. The explanation of this seemingly unexpected effect is in fact in line within the RC model we propose as follows. The current applied, which would flow through the entire 3D LCMO single-layer film, flows through one (or a few) top 2D layers in the SL, implying higher E in each of them across all possible barriers, such as domain boundaries, phase separation within domains, *etc*. Higher E suggests easier mutual phase charging followed by the corresponding easier discharging and formation of additional conducting filaments between phases, domains, *etc*. This obviously leads to lower resistivity in the SL than in the LCMO films with tunneling-driven conductivity across all possible barriers. In general, this process is likely to be responsible for the presence (controllability) of the sharp resistivity drops. However, we should mention that the difference in resistivity can also be influenced by (i) the oxygen content in LCMO,[18,19] which (ii) may not be reproduced by PLD without the due attention, which (iii) may be affected by the proximity of the interlayers and interfaces (also reducing surface conductivity noticed upon SEM studies), and (iv) by the loss of oxygen during gold contact deposition, which (v) may be different for the films and SL.

The recent theoretical study has demonstrated[23] that in the vicinity of region of competition between the ferromagnetic metallic and spin-charge-ordered insulating phases, the CMR phenomenon may be observed with MR of up to 10000% with the resistivity behavior becoming metallic *via* an abrupt discontinuity. We indeed observe large MR in excess of ~2000% in the form of discontinuities, likely representing the dimensional or a first-order transition. It is the sharpest, strongest, and, importantly, controlled MR behavior reported in LCMO films and superlattices.[31]

CONCLUSION

In summary, we have manufactured LCMO films and LCMO/STO superlattices by PLD and investigated their properties by means of magnetic and transport measurements. We have managed to establish an acceptable technology for combination of LCMO films exhibiting the CMR effect with HTS REBCO films for novel hybrid functionalities and devices, so that the relevant magnetic properties of LCMO at $T < T_C$ would

be exhibited below the superconducting transition temperature. This can be achieved by reducing thickness of LCMO single-layer films but more *effectively and controllably* by introducing LCMO/STO superlattices with the period of $n > 20$ and 3−7 nm thick layers. We have obtained $T_C \simeq 74$ K, which is even below liquid nitrogen temperature (and $T_C \simeq 91$ K of HTS REBCO films), enabling an easier cooling approach for potential applications. A shift of the metal−insulator transition to lower temperatures in $\rho(T)$ curves has been also observed for the films and superlattices. Importantly, the $\rho(T)$ curves of the superlattices below the MIT have remarkable sharp features exhibiting about 2 orders of magnitude drops of resistivity, which result in the positive peak of magnetoresistance in excess of 2000% at 75 K. We have explained this behavior in the framework of the phase separation theory for manganites for the well-organized 3D structures, which experience dimensional transitions of their spin-charge transport properties. The significant result is that, because the structure of the superlattices can be easily controlled, it can enable the prescribed tuning of the magnetoresistance properties required for applications. Moreover, the dimensionality-dependent behavior observed and its magnetic field dependence indicate the presence of magnetodielectric properties in STO layers. The variety of the new technological and fundamental results obtained in this work is applicable to a broad range of adjoining scientific areas.

EXPERIMENTAL DETAILS

Thin films of $La_{2/3}Ca_{1/3}MnO_3$, $SrTiO_3$ (STO), and their heterostructures were epitaxially deposited on 5×5 mm^2 STO(100) and $LaAlO_3$ (LAO) substrates by a standard PLD technique developed and employed for high-quality $YBa_2Cu_3O_7$ film deposition[32] with a pulsed KrF excimer laser (wavelength of 248 nm) at the laser fluency of ∼3−4 J/cm^2 and the pulse repetition rate of 5 Hz. The oxygen pressure in the vacuum chamber was maintained at 300 mTorr during all deposition processes. The target to substrate distance was typically 65−70 mm with each target rotating uniformly around their axes in order to obtain homogeneous high-quality epitaxial films. The deposition temperature was kept at 780 °C for all materials used. The thickness of epitaxial layers was controlled by the deposition rate determined by measuring thickness with the help of surface profiler measurements. The programmable target carousel was used to facilitate the noninterrupting deposition process for manufacturing multilayered structures and superlattices. Magnetic measurements were performed using a superconducting quantum interference device (MPMS) by Quantum Design. The surface morphology of thin film was investigated using a field emission scanning electron microscope (SEM) equipped with a through the lens (TTL) detector. The interfaces between layers and microstructure of the superlattices were observed by transmission electron microscopy (TEM), as well as energy-filtering transmission electron microscopy (not shown). Cross-sectional TEM samples were prepared using lift-off focused ion beam technique. For magneto-transport measurements, golden contact pads were deposited by laser ablation. The sample resistance as a function of temperature and current−voltage (*IV*) characteristics was measured by a dc four-probe method at different applied magnetic fields.

Conflict of Interest: The authors declare no competing financial interest.

Acknowledgment. This work is financially supported by the Australian Research Council.

REFERENCES AND NOTES

1. von Helmholt, R.; Wecker, J.; Holzapfel, B.; Schultz, L.; Samwer, K. Giant Negative Magnetoresistance in Perovskitelike $La_{2/3}Ba_{1/3}MnO_x$ Ferromagnetic Films. *Phys. Rev. Lett.* **1993**, *71*, 2331.
2. Jin, S.; Tiefel, T. H.; McCormack, M.; Fastnacht, R. A.; Ramesh, R.; Chen, L. H. Thousandfold Change in Resistivity in Magnetoresistive La-Ca-Mn-O Films. *Science* **1994**, *264*, 413.
3. Hoppler, J.; Stahn, J.; Niedermayer, Ch.; Malik, V. K.; Bouyanfif, H.; Drew, A. J.; Rossle, M.; Buzdin, A.; Cristiani, G.; Habermeier, H. U.; *et al.* Giant Superconductivity-Induced Modulation of the Ferromagnetic Magnetization in a Cuprate-Manganite Superlattice. *Nat. Mater.* **2009**, *8*, 315.
4. Fedoseev, S. A.; Pan, A. V.; Shcherbakova, O. V.; Dou, S. X. Electroresistance and Magnetoresistance Effects in Superconductor-Insulator-Ferromagnet Hybrid Structures. *Physica C* **2012**, *479*, 143–146.
5. Dörr, K.; De Teresa, J. M.; Müller, K.-H.; Eckert, D.; Walter, T.; Vlakhov, E.; Nenkov, K.; Schultz, L. Preparation and Properties of Epitaxial $La_{0.7}Ca_{0.3}MnO_3$ Films with Reduced Carrier Density. *J. Phys.: Condens. Matter* **2000**, *12*, 7099–7109.
6. Nagaev, E. L. Phase Separation in Degenerate Magnetic Oxide Semiconductors. *Phys. Solid State* **1998**, *40*, 1873–1877.
7. Chen, S. F.; Lin, P. I.; Juang, J. Y.; Uen, T. M.; Wu, K. H.; Gou, Y. S.; Lin, J. Y. Metallic Percolation in $La_{0.67}Ca_{0.33}MnO_3$ Thin Films. *Appl. Phys. Lett.* **2003**, *82*, N8.
8. Tao, J.; Niebieskikwiat, D.; Varela, M.; Luo, W.; Schofield, M.; Zhu, Y.; Salamon, M. B.; Zuo, J. M.; Pantelides, S. T.; Pennycook, S. J. Direct Imaging of Nanoscale Phase Separation in $La_{0.55}Ca_{0.45}MnO_3$: Relationship to Colossal Magnetoresistance. *Phys. Rev. Lett.* **2009**, *103*, 097202.
9. Markovich, V.; Jung, G.; Yuzhelevskii, Y.; Gorodetsky, G.; Gao, J. Metastable Resistivity of LaCaMnO Manganite Thin Films. *Phys. Rev. B* **2007**, *75*, 104419.
10. Zhai, H.; Ma, J. X.; Gillaspie, D. T.; Zhang, X. G.; Ward, T. Z.; Plummer, E. W.; Shen, J. Giant Discrete Steps in Metal-Insulator Transition in Perovskite Manganite Wires. *Phys. Rev. Lett.* **2006**, *97*, 167201.
11. Deen, P. P.; Yokaichiya, F.; de Santis, A.; Bobba, F.; Wildes, A. R.; Cucolo, A. M. Ferromagnetic Clusters and Superconducting Order in $La_{0.7}Ca_{0.3}MnO_3/YBa_2Cu_3O_7$ Heterostructures. *Phys. Rev. B* **2006**, *74*, 224414.
12. Dvorak, J.; Idzerda, Y. U.; Ogale, S. B.; Shinde, S.; Wu, T.; Venkatesan, T.; Godfrey, R.; Ramesh, R. Are Strain-Induced Effects Truly Strain Induced? A Comprehensive Study of Strained LCMO Thin Films. *J. Appl. Phys.* **2005**, *97*, 10.
13. Kwon, C.; Kim, K. C.; Robson, M. C.; Gu, J. Y.; Rajeshwari, M.; Venkatesan, T.; Ramesh, R. Desirable Magnetotransport Properties in Doped Mn-Oxide-Based Superlattices. *J. Appl. Phys.* **1997**, *81*, 4950–4952.
14. Jo, M.; Mathur, N. D.; Evetts, J. E.; Blamire, M. G. Magnetotransport and Interface Magnetism in Manganite Heterostructures: Implication for Spin Polarized Tunnelling. *Mater. Res. Soc. Symp. Proc.* **1999**, *602*, 3.
15. Pan, A. V.; Pysarenko, S. V.; Wexler, D.; Rubanov, S.; Dou, S. X. Multilayering and Ag-Doping for Properties and Performance Enhancement in $YBa_2Cu_3O_7$ Films. *IEEE Trans. Appl. Supercond.* **2007**, *17*, 3585.
16. Pan, V. M.; Pan, A. V. Vortex Matter in Superconductors. *Fiz. Niz. Temp. (Rus.)* **2001**, *27*, 991; *Low Temp. Phys.* **2001**, *27*, 732.
17. Pan, V. M.; Cherpak, Y.; Komashko, V.; Pozigun, S.; Tretiatchenko, C.; Semenov, A.; Pashitskii, E.; Pan, A. V. Supercurrent Transport in $YBa_2Cu_3O_{7-\delta}$ Epitaxial Thin Films in a dc Magnetic Field. *Phys. Rev. B* **2006**, *73*, 054508.

18. Ziese, M.; Semmelhack, H. C.; Han, K. H. Strain-Induced Orbital Ordering in Thin $La_{0.7}Ca_{0.3}MnO_3$ Films on $SrTiO_3$. *Phys. Rev. B* **2003**, *68*, 134444.
19. Guo, H. Z.; Gupta, A. J.; Zhang, J.; Varela, M.; Pennycook, S. J. Effect of Oxygen Concentration on the Magnetic Properties of La_2CoMnO_6 Thin Films. *Appl. Phys. Lett.* **2007**, *91*, 202509.
20. Lee, Y. P.; Park, S. Y.; Park, J. S.; Prokhorov, V. G.; Komashko, V. A.; Svetchnikov, V. L.; Kang, J.-H. Magnetic Phase Diagram and Structural Separation of $La_{0.7}(Ca_{1-y}Sr_y)_{0.3}MnO_3$ Thin Films. *J. Appl. Phys.* **2007**, *101*, 053708.
21. Shang, D. S.; Chen, L. D.; Wang, Q.; Yu, W. D.; Li, X. M.; Sun, J. R.; Shen, B. G. Crystallinity Dependence of Resistance Switching in $La_{0.7}Ca_{0.3}MnO_3$ Films Grown by Pulsed Laser Deposition. *J. Appl. Phys.* **2009**, *105*, 063511.
22. Nigam, R.; Pan, A. V.; Dou, S. X. Explanation of Magnetic Behavior in Ru-Based Superconducting Ferromagnets. *Phys. Rev. B* **2008**, *77*, 134509.
23. Sen, C.; Alvarez, G.; Dagotto, E. First Order Colossal Magnetoresistance Transitions in the Two-Orbital Model for Manganites. *Phys. Rev. Lett.* **2010**, *105*, 097203.
24. Sawa, A. Resistive Switching in Transition Metal Oxides. *Mater. Today* **2008**, *11*, issue 6.
25. Infante, I. C.; Sanchez, F.; Fontcuberta, J.; Fusil, S.; Bouzehouane, K.; Herranz, G.; Barthelemy, A.; Estrade, S.; Arbiol, J.; Peiro, F.; *et al.* Structural and Functional Characterization of (110)-Oriented Epitaxial $La_{2/3}Ca_{1/3}MnO_3$ Electrodes and $SrTiO_3$ Tunnel Barriers. *J. Appl. Phys.* **2007**, *101*, 093902.
26. Boikov, Yu. A.; Danilov, V. A. Reaction of LCMO Films Electroresistance on the Increasing in the Film-Substrate Lattice Mismatch. *Zh. Tekh. Fiz.* **2005**, *31*, 73; *Tech. Phys. Lett.* **2005**, *31*, 36.
27. Boikov, Yu. A.; Danilov, V. A. Response of the Capacitance of a Planar $La_{0.67}Ca_{0.33}MnO_3/SrTiO_3/La_{0.67}Ca_{0.33}MnO_3$ Heterostructure to an Electric Field. *Phys. Solid State* **2010**, *52*, 1439–1443.
28. Kolodiazhnyi, T.; Fujita, K.; Wang, L.; Zong, Y.; Tanaka, K.; Sakka, Y.; Takayama-Muromachi, E. Magnetodielectric Effect in $EuZrO_3$. *Appl. Phys. Lett.* **2010**, *96*, 252901.
29. Choudhury, D.; Mukherjee, S.; Mandal, P.; Sundaresan, A.; Waghmare, U. V.; Bhattacharjee, S.; Mathieu, R.; Lazor, P.; Eriksson, O.; Sanyal, B.; *et al.* Tuning of Dielectric Properties and Magnetism of $SrTiO_3$ by Site-Specific Doping of Mn. *Phys. Rev. B* **2011**, *84*, 125124.
30. Rivas, J.; Mira, J.; Rivas-Murias, B.; Fondado, A.; Dec, J.; Kleemann, W.; Señarís-Rodríguez, M. A. Magnetic-Field-Dependent Dielectric Constant in $La_{2/3}Ca_{1/3}MnO_3$. *Appl. Phys. Lett.* **2006**, *88*, 242906.
31. Fei, L.; Zhu, L.; Cheng, X.; Wang, H.; Baber, S. M.; Hill, J.; Lin, Q.; Xu, Y.; Deng, S.; Luo, H. Structure and Magnetotransport Properties of Epitaxial Nanocomposite $La_{0.67}Ca_{0.33}MnO_3$:$SrTiO_3$ Thin Films Grown by a Chemical Solution Approach. *Appl. Phys. Lett.* **2012**, *100*, 082403.
32. Pan, A. V.; Pysarenko, S.; Dou, S. X. Drastic Improvement of Surface Structure and Current-Carrying Ability in $YBa_2Cu_3O_7$ Films by Introducing Multilayered Structure. *Appl. Phys. Lett.* **2006**, *88*, 232506.